1989ApJ...337..691K

THE ASTROPHYSICAL JOURNAL, 337:691–703, 1989 February 15
© 1989. The American Astronomical Society. All rights reserved. Printed in U.S.A.

HIGH-RESOLUTION CO OBSERVATIONS OF NGC 1068[1]

NOBORU KANEKO AND KAZUHIKO MORITA
Department of Physics, Hokkaido University

YASUO FUKUI, KOJI SUGITANI, AND TAKAHIRO IWATA
Department of Astrophysics, Nagoya University

NAOMASA NAKAI AND NORIO KAIFU
Nobeyama Radio Observatory, University of Tokyo

AND

HARVEY S. LISZT
National Radio Astronomy Observatory
Received 1988 February 22; accepted 1988 August 3

ABSTRACT

High-resolution ^{12}CO $J = 1$–0 line observations of the 60″ × 60″ disk of NGC 1068 have been made using the Nobeyama 45 m telescope (HPBW = 17″). The integrated CO map reveals three major components: (1) *a disk component* of 40″ × 60″ elongated along a northeast-southwest direction, (2) *a northeast component* located in a dusty area between the east inner spiral and the nuclear region, and (3) *a southwest component* located in a dusty region connecting a south bay held between the central inner region and the southwest H II region and a heavily obscured red portion lying on the west inner spiral. The disk component, which closely matches the region of red colors outside the inner arm region, coincides with the radio plateau and the 100 μm far-infrared source. Excellent correspondence is also found between the northeast and southwest components and the 10 μm infrared emission. That NGC 1068 has no nuclear component of CO is confirmed, which suggests an indirect relation between the nuclear and the star-forming activities of NGC 1068. The total H_2 mass is estimated to be $5.6 \times 10^9\ M_\odot$. The diagram of isovelocity contours shows a peculiar structure in that the isovelocity contours primarily run parallel to the north-south direction. If this velocity structure is due to a circular motion of the disk, the position angle of 82° is suggested for the kinematic major axis, which is consistent with recent optical observations. However, the isovelocity contour map cannot be explained only in terms of a circular motion, which indicates that there are large-scale noncircular motions in the CO molecular gas within the 1′ × 1′ disk of NGC 1068.

Subject headings: galaxies: individual (NGC 1068) — galaxies: Seyfert — interstellar: molecules

I. INTRODUCTION

Since the detection of intense CO emission by Rickard *et al.* (1977), the Seyfert galaxy NGC 1068 has been of particular interest as a typical example of superluminous starburst galaxies. It was originally classified as a prototype of type 2 Seyfert galaxies (Khachikian and Weedman 1971; Weedman 1973) and recently was found to have broad wings characteristic of type 1 Seyferts (Antonucci and Miller 1985; Snijders, Netzer, and Boksenberg 1986).

The fact that star formation is enhanced in the extranuclear region of NGC 1068 is indicated directly or indirectly by its peculiar morphologies: unusually bright inner spiral arms (Sandage 1961; Walker 1968; Keel and Weedman 1978; Snijders, Briggs, and Boksenberg 1982), prominent dust lanes (Sandage 1961), knotty structures due to H II regions and dust patches (Arp 1966; Ichikawa *et al.* 1987), abnormally blue colors of the disk (Smith, Weedman, and Spinrad 1972; Schild, Tresch-Fienberg, and Huchra 1985; Ichikawa *et al.* 1987), and the presence of extended emission lines (Nishimura, Kaneko, and Toyama 1984; Balick and Heckman 1985; Evans and Dopita 1986, 1987). Examination of the above data, together with radio continuum (Wilson and Ulvestad 1982; Wynn-Williams, Becklin, and Scoville 1985), infrared (Telesco and Harper 1980; Telesco *et al.* 1984), and CO (Scoville, Young, and Lucy 1983) observations reveal that bursts of star formation have occurred widely in a disk region of about 1′ diameter.

The CO emission serves as a good tracer of molecular gas, which is a fuel of star formation in starburst galaxies, and a precise knowledge of the spatial distribution and dynamics of CO molecular clouds in the central 1′ of NGC 1068 is very important to understanding the nuclear and star-forming activities that take place in this galaxy and other galaxies having both Seyfert and starburst characteristics. Scoville, Young, and Lucy (1983) have tried to map the ^{12}CO $J = 1$–0 emission in the central region of NGC 1068 by applying the kinematic rectification scheme on the CO line profiles measured at 22″ spacing with the FCRAO 14 m telescope, with a resolution of 50″ (HPBW). The result reveals two components: (1) a molecular cloud ring corresponding to the optically bright inner spirals at $R \sim 15''$ which contains one-third of the total CO emission, and (2) a uniform component containing two-thirds of the total emission. The total mass of $6 \times 10^9\ M_\odot$ was estimated for molecular clouds inside 30″ radius. Myers and Scoville (1987) recently published a high-resolution map of NGC 1068 obtained with the Owens Valley Millimeter Interferometer at 6″ angular resolution, which shows an incomplete molecular ring located on the outer edge of the inner arm

[1] This work was carried out under the common use observation program at Nobeyama Radio Observatory (NRO). Nobeyama Radio Observatory, a branch of the Tokyo Astronomical Observatory, University of Tokyo, is a cosmic radio observing facility open to outside users.

© American Astronomical Society • Provided by the NASA Astrophysics Data System

1989ApJ...337..691K

region. In these two observations, no evidence is found for a nuclear component.

In this paper we present high-resolution CO observations of the 60″ × 60″ disk of NGC 1068 made with the NRO 45 m telescope. Our large filled aperture measurements may provide more precise information on the global structure and velocity field of CO molecular clouds for NGC 1068. In § II, CO observations of NGC 1068 are described. Intensity and velocity structures of CO emission, and H_2 mass are given in § III. Section IV is devoted to comparison with the interferometer observations of Myers and Scoville (1987) and radio and infrared observations. Velocity field and a CO line-width map are also discussed.

II. OBSERVATIONS

The CO observations of NGC 1068 were made in 1985 April and 1986 April using the 45 m telescope of the Nobeyama Radio Observatory. The receiver front end was a cooled Schottky mixer-receiver. The system noise temperature (SSB) at the ^{12}CO $J = 1$–0 frequency (115.271204 GHz), including the atmospheric effect and the antenna ohmic loss, was 600–800 K. The spectra were taken with the 2048 channel wide-band acousto-optical spectrometer, which provided an instantaneous bandwidth of 256 MHz (666 km s^{-1}). The frequency resolution was 250 kHz, corresponding to a velocity resolution of 0.65 km s^{-1}. The full half-power beamwidth (HPBW) was 17″, which corresponds to 1.5 kpc at a distance of 18.1 Mpc (Sandage and Tammann 1975). The aperture efficiency η_a and the main-beam efficiency η_{mb} were measured to be 0.26 and 0.45, respectively, using Venus, Mars, and Saturn.

The observations were made in position-switching mode. In one cycle of the switching observations, one OFF position was observed after observing one to three different ON positions to obtain more points within the observing time allowed while keeping the good signal-to-noise ratio. At each position the signal was integrated for 20 s (on source) every cycle, and typically 20 cycles were repeated. The pointing was carefully calibrated by observing the SiO maser source *o* Cet (ΔR.A. = -0^h23^m, Δdecl. = $-3°$ from NGC 1068) every hour. The absolute pointing accuracy was estimated to be better than 4″. The calibration of line intensity was done using an absorbing chopper in front of the receiver. The intensity scale is the antenna temperature, T_A^*, corrected for the atmospheric and antenna ohmic losses (Ulrich and Haas 1976) but not for the beam efficiency.

Figure 1 shows the 56 positions where CO observations were made, superposed on the isophotes in the *B* band. In the central 30″ × 30″ (2.6 × 2.6 kpc) including luminous ringlike inner spirals, CO spectra were fully sampled at 25 positions spaced by 7.″5 (0.66 kpc), while in the 60″ × 60″ (5.2 × 5.2 kpc) disk outside the central region 28 positions were selected with spacings of 15″, so that no positions are lacking on either the northeast-southwest or the southeast-northwest directions. In addition to the above 53 positions, CO spectra were also observed at three positions (37.″5 west, 7.″5 south), (37.″5 west, 22.″5 south), and (37.″5 west, 37.″5 south). The parameters adopted for NGC 1068 are listed in Table 1.

III. RESULTS

The CO line parameters measured at each position are summarized in Table 2. The CO spectra obtained are shown in Figure 2, where data are smoothed to 21 km s^{-1} resolution. The (0″, 0″) position corresponds to that of the optical nucleus (Clements 1981). For a systemic velocity of NGC 1068 we adopt v_{LSR}(CO) = 1123 ± 4 km s^{-1}, the weighted mean velocity calculated from all of the mean velocities and integrated intensities measured at 47 positions which are symmetric with respect to the center.

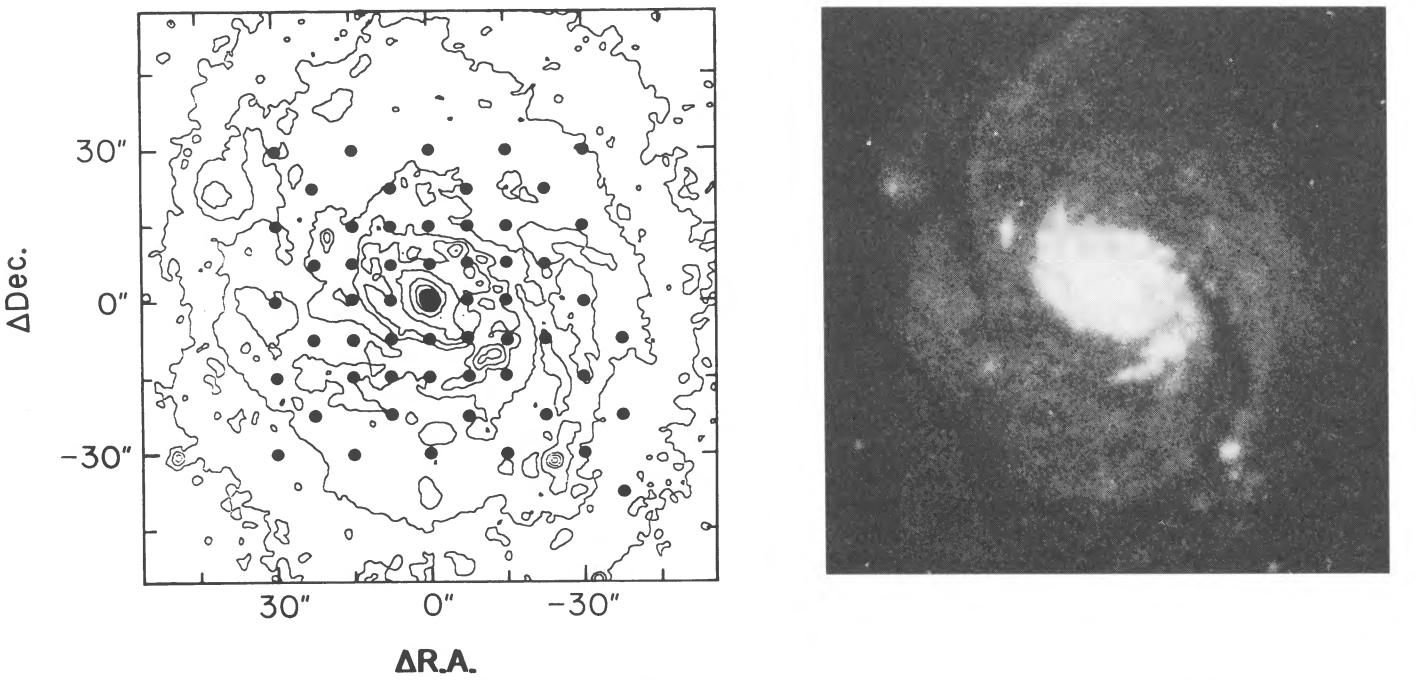

FIG. 1.—Observed points superposed on the isophotes, and the photograph of NGC 1068 in the *B* band. The isophotes are drawn using the data set of Ichikawa *et al.* (1987). The blue photograph was obtained by one of the authors (N. K.) and M. Nishimura and K. Toyama, with the Okayama 188 cm reflector on 103a-O with an L39 filter.

© American Astronomical Society • Provided by the NASA Astrophysics Data System

1989ApJ...337..691K

TABLE 1

PARAMETERS OF NGC 1068

Parameter	Value
R.A. (1950)[a]	$02^h40^m07^s.076$
Decl. (1950)[a]	$-00°13'31''.48$
Systemic velocity[b]	1123 ± 4 km s^{-1}
Distance[c]	18.1 Mpc
Inclination[d]	37°
Position angle of major axis[e]	$82° \pm 2°$
Beam size on galaxy (17″)	1.5 kpc

[a] Clements 1981.

[b] Velocity relative to the local standard of rest (LSR) determined from the weighted mean of the mean CO velocities at 47 positions which are symmetric with the center. This corresponds to $v_\odot = 1134$ km s^{-1}.

[c] Sandage and Tammann 1975.

[d] Determined from the axial ratio of the envelope of NGC 1068 ($b/a = 0.78$–0.82), using the photographs obtained with the Kiso Schmidt telescope.

[e] Position angle of the kinematic major axis determined from the CO isovelocity contour map. The Kiso Schmidt photographs give p.a. = 85° for the major axis.

a) *Intensity Structure*

Figure 3 shows the contour map of the integrated CO intensity $I_{CO} = \int T_A^* dv$ in the central $\sim 1'$ of NGC 1068. Figure 4 is the same map superposed on the U-band isophotes of the inner arm region. The intensity map exhibits the disklike distribution of CO with a spatial extent of 40″ × 60″ (3.5 × 5.2 kpc) elongated along a northeast-southwest direction, and two peaks at $\sim 10''$ northeast and $\sim 15''$ southwest from the center. Hereafter, they are referred to as the *disk*, *northeast*, and *southwest components*, respectively. Figure 3 is different from the results of Myers and Scoville (1987), and comparison with the latter will be discussed in § IV*a*.

Analysis of the radial distribution of the CO intensity (Table 2) reveals that the disk component is *a plateau* rather than a ring. Our disk component would correspond to a disk component suggested by Blitz, Mathieu, and Bally (1986). Comparison with the two-dimensional color distributions shown in Figures 2*e* and 2*f* of Ichikawa *et al.* (1987) shows that the disk component coincides well with regions of redder color outside the inner arm region. In § IV*b* we shall compare the disk component with the distributions of the radio continuum and infrared emission. We note that, although the CO intensity decreases outside the disk component, there is still detectable CO emission even at the outermost positions observed ($R \geq 30''$–$40''$), which implies that, in addition to the disk component, there is an extended component in the outer disk.

Comparison with the superposed isophotes (Fig. 4) shows that the northeast component, which has a peak at the position (7″.5 east, 7″.5 north), coincides well with a dusty area between the east inner spiral arm and the nuclear region (also see Fig. 2*d* of Ichikawa *et al.* 1987). An extension of the northeast component at (22″.5 east, 22″.5 north) also lies on a dusty area between the inner and main spirals. On the other hand, the southwest component, whose peak is found at the position (7″.5 west, 15″ south), has structures elongated along a northward direction, and is located on a dusty area between the nuclear region and the west inner spiral arm. The southwest component also shows a westward protrusion at (15″ west, 7″.5 south), corresponding to a heavily obscured region (see Arp 1966 and Fig. 2*a* of Ichikawa *et al.* 1987) which divides the west inner spiral arm into two northwest and southwest portions, and closely matches the position of the maximum peak temperature.

Thus, we see that all of the major CO components derived above coincide very well with dusty red areas, and that no strong CO emission is found in optically bright northwest H II complexes (knot 5 of Schild, Tresch-Fienberg, and Huchra 1985) located on the northwest inner spiral and southwest H II region (knot 3 of Schild, Tresch-Fienberg, and Huchra 1985) lying on the southwest inner spiral. This implies that in the central $\sim 1'$ of NGC 1068 most of the molecular gas is associated not with ionized gaseous clouds within the inner spirals but with dust clouds embedded within the optically obscured regions of red colors.

As can be seen in Figure 3, our single-dish CO observations (17″ HPBW) resolve no nuclear component, consistent with the results obtained by Scoville, Young, and Lucy (1983) and Myers and Scoville (1987). The fact that NGC 1068, whose nucleus is very active in the optical and infrared, has no prominent nuclear component of CO emission seems to suggest no direct relation between the nuclear activity and the star-forming activity taking place within the central $\sim 1'$.

b) *Velocity Structure*

The contour diagrams of peak and mean velocities are presented in Figures 5 and 6, respectively. As can be seen in Figure 2, some CO profiles are strongly asymmetric with respect to the mean velocities, and our single-dish observations were made with a 17″ beam, which is considerably larger than our spacings. Therefore, in the following, we analyze the contour diagram of peak velocities (Fig. 5). Comparison shows that the velocity structures in Figures 5 and 6 are quite similar, and the results obtained in the following are valid for Figure 6.

The isovelocity contours of 1100–1160 km s^{-1} penetrate both the nucleus and the brightest knot of northwest H II complexes, and the isovelocity contours of 1020–1080 km s^{-1}, which are passing through the nuclear region, bend eastward both on the north and on the south. The region of lowest velocities ($v_{LSR} < 1020$ km s^{-1}) is limited to a fanlike east area. A northward protrusion of the contour of 1020 km s^{-1} at (10″ east, 5″ north) to (10″ east, 20″ north) may be due to the presence of low-velocity CO clouds associated with the northeast component. Similarly, eastward protrusions of the isovelocity contours of 1220 and 1240 km s^{-1} at (20″ west, 0″ north) to (10″ west, 5″ south) indicate the presence of high-velocity CO clouds within the southwest component. A low-velocity region encircled by the contour of 1200 km s^{-1}, whose center is at (22″ west, 22″ south), is located on the prominent dust lane (Sandage 1961). That the isovelocity contours are deformed in the areas of the northeast and southwest components is the evidence for the deviation of their velocities from a circular motion.

The remarkable feature of Figure 5 is that the isovelocity contours primarily run parallel to the north-south direction. Most of the velocities measured on the east side (ΔR.A. $\geq 15''$) are nearly constant within a small range, and their weighted mean is estimated to be 1024 ± 5 km s^{-1}, where weighting is proportional to the observed antenna peak temperature at each position. A similar tendency is seen for the velocities observed on the west side (ΔR.A. $\leq -15''$), and their weighted mean is evaluated as 1226 ± 5 km s^{-1}. If the velocity structure is due primarily to a circular motion of the disk, we find the position angle of 82° for a kinematic major axis, which just

© American Astronomical Society • Provided by the NASA Astrophysics Data System

1989ApJ...337..691K

TABLE 2

CO LINE PARAMETERS

NUMBER	POSITION (1950) R.A. (arcsec)	Decl. (arcsec)	T_A^*(peak) (K)	I_{CO} (K km s^{-1})	V_{peak}[a] (km s^{-1})	V_{mean}[a] (km s^{-1})	V_{FWHM}[b] (km s^{-1})
1	30	30	0	−0.7	...	...	...
2	30	15	0.23	19.4	1070	1052	84
3	30	0	0.22	25.2	1005	1045	114
4	30	−15	0.10	7.8	1000	1039	78
5	30	−30	0.14	16.8	1020	1094	120
6	22.5	22.5	0.29	33.4	1025	1061	115
7	22.5	7.5	0.35	31.1	1005	1032	89
8	22.5	−7.5	0.17	17.8	1000	1045	105
9	22.5	−22.5	0.11	13.8	1030	1081	125
10	15	30	0.13	16.8	1045	1083	129
11	15	15	0.30	36.4	1025	1067	121
12	15	7.5	0.46	45.2	1025	1042	98
13	15	0	0.37	38.2	1005	1055	103
14	15	−7.5	0.36	41.6	1005	1049	115
15	15	−15	0.19	37.8	1010	1103	199
16	15	−30	0.17	22.6	1055	1081	133
17[c]	7.5	22.5	0.18[d] 0.21	31.1	1000[d] 1105	1073	173[d] 148
18[c]	7.5	15	0.24[d] 0.22	42.3	1000[d] 1100	1081	176[d] 192
19[c]	7.5	7.5	0.33[d] 0.29	60.9	1000[d] 1105	1100	184[d] 210
20	7.5	0	0.40	52.0	1015	1067	130
21	7.5	−7.5	0.37	44.1	1025	1057	119
22	7.5	−15	0.30	36.5	1010	1020	122
23	7.5	−22.5	0.20	28.7	1055	1086	143
24	0	30	0.21	15.0	1075	1086	71
25[c]	0	15	0.24 0.28[d]	46.3	1050 1110[d]	1103	193 165[d]
26[c]	0	7.5	0.18[d] 0.27	40.7	1030[d] 1110	1116	226[d] 151
27[c]	0	0	0.18 0.21[d]	42.9	1030 1110[d]	1125	238 204[d]
28	0	−7.5	0.30	44.7	1090	1096	149
29	0	−15	0.24	39.4	1130	1118	164
30	0	−30	0.13	17.3	1195	1200	133
31	−7.5	22.5	0.14	12.7	1180	1154	91
32	−7.5	15	0.26	38.7	1190	1166	149
33	−7.5	7.5	0.25	36.5	1180	1169	146
34	−7.5	0	0.27	60.8	1230	1169	225
35	−7.5	−7.5	0.30	65.7	1230	1168	219
36	−7.5	−15	0.40	66.0	1195	1162	165
37	−7.5	−22.5	0.20	25.0	1180	1165	125
38	−15	30	0	0.8	...	...	...
39	−15	15	0.30	34.7	1200	1218	116
40	−15	7.5	0.33	28.3	1205	1212	86
41	−15	0	0.30	27.7	1250	1195	92
42	−15	−7.5	0.43	44.0	1230	1213	102
43	−15	−15	0.32	27.7	1225	1218	86
44	−15	−30	0.20	28.1	1220	1219	140
45	−22.5	22.5	0.10	11.2	1220	...	112
46	−22.5	7.5	0.30	26.1	1225	1229	87
47	−22.5	−7.5	0.29	27.7	1250	1256	95
48	−22.5	−22.5	0.22	23.0	1185	1162	104
49	−30	30	0.08	6.8	1230	1228	85
50	−30	15	0.16	12.4	1240	1236	77
51	−30	0	0.29	21.8	1250	1240	75
52	−30	−15	0.25	18.3	1245	1241	73
53	−30	−30	0.17	14.4	1215	1207	85
54	−37.5	−7.5	0.21	22.0	1255	1234	105
55	−37.5	−22.5	0.17	16.5	1200	1213	97
56	−37.5	−37.5	0.16	22.0	1190	1195	137

© American Astronomical Society • Provided by the NASA Astrophysics Data System

1989ApJ...337..691K

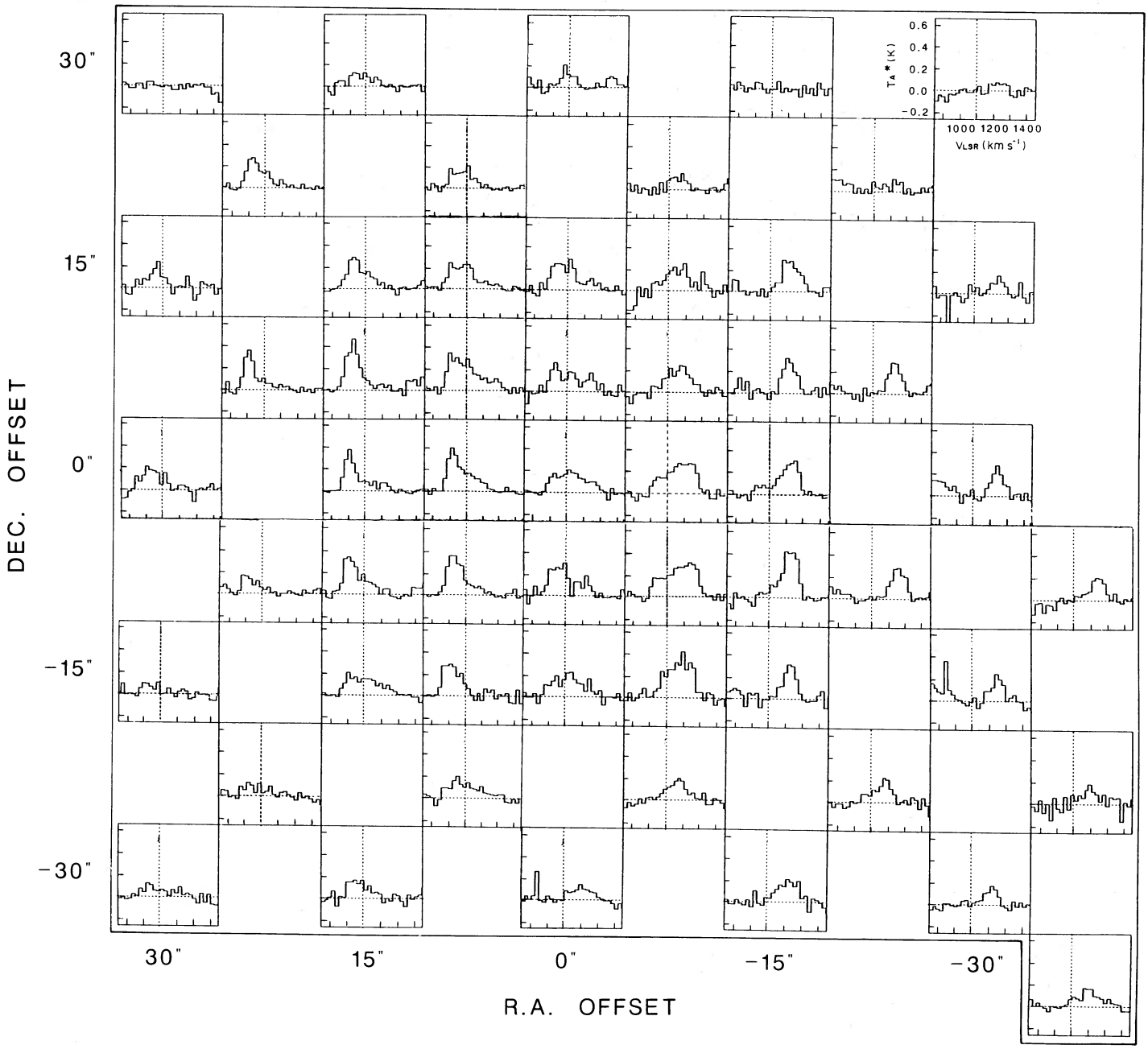

FIG. 2.—Fifty-six spectra of the CO line obtained for NGC 1068 at 7".5 or 15" intervals. The (0", 0") position corresponds to the optical center of NGC 1068 (Clements 1981). The abscissa of each box is the antenna temperature T_A^* in K. The ordinate is the LSR velocity (850–1450 km s^{-1}). The dotted vertical line indicates 1100 km s^{-1}. Each spectrum is smoothed to 21 km s^{-1}.

NOTES TO TABLE 2

[a] Velocities are with respect to the local standard of rest (LSR).

[b] The full width at half-intensity is defined by $V_{FWHM} = I_{CO}/T_A^*$(peak).

[c] Double peak.

[d] Value adopted in drawing figures.

© American Astronomical Society • Provided by the NASA Astrophysics Data System

1989ApJ...337..691K

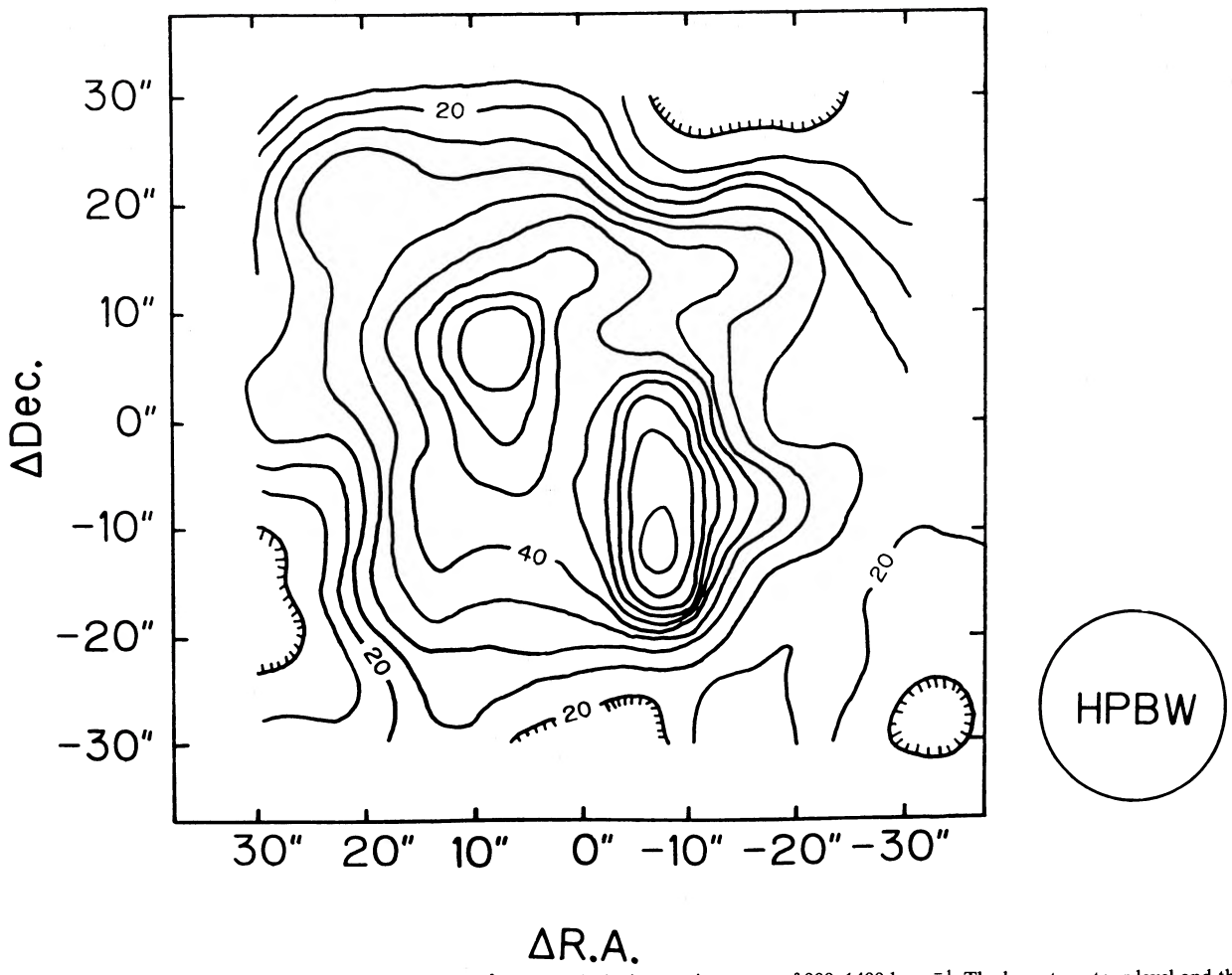

FIG. 3.—Map of the integrated intensity of the CO emission, $\int T_A^* dv$, with the integration range of 900–1400 km s^{-1}. The lowest contour level and the contour interval are 5 K km s^{-1}. The HPBW (17″) of the telescope is denoted by a circle at the lower right.

agrees with the kinematic position angle determined from the Hα velocity map of Atherton, Reay, and Taylor (1985) by Myers and Scoville (1987). According to optical observations of Baldwin, Wilson and Whittle (1987), the position angle of the kinematic major axis lies within 80° ± 9°. The kinematic major-axis position angle of 82° is also consistent with that deduced from H I observations (Heckman, Balick, and Sullivan 1978; Baan and Haschick 1983) and the position angle of the major axis of the outer envelope (Table 1). If the true position angle of the kinematic major axis of NGC 1068 is close to 82°, and if the main disk is coplanar with the outer envelope, the main disk would have a barlike structure.

Figure 7 shows the position-velocity map of p.a. = 90°, which is very near the major axis. Low- and high-velocity peaks are found at v_{LSR} = 1005 and 1240 km s^{-1}, respectively. The figure exhibits a flat rotation curve, and the maximum circular velocity estimated at the level 20% of peak is about 160 km s^{-1}, which corresponds to 266 km s^{-1} after the correction for the galaxy inclination of i = 37° (Table 1). This is consistent with the maximum rotation velocities 144–330 km s^{-1} for Sb galaxies (Rubin *et al.* 1982, 1985). By adopting a smaller inclination of i = 19°, Baldwin, Wilson, and Whittle (1987) have derived a circular velocity about twice as large as the one we determined.

c) H_2 *Mass*

In order to estimate the molecular mass, we adopt an empirical relation obtained for molecular clouds in our Galaxy (Young and Scoville 1982):

$$N_{H_2} = 4 \times 10^{20} (\cos i) \int T_A^* dv \ H_2 \ \mathrm{cm}^{-2} , \qquad (1)$$

where i is the galaxy inclination. The resultant column densities N_{H_2} are 2.3 × 10^{22}(cos i) H_2 cm^{-2} and 2.7 × 10^{22}(cos i) H_2 cm^{-2} for the northeast and southwest peaks, respectively. The column density of the disk component ($R \lesssim 2.2$ kpc) is about 1.6 × 10^{22}(cos i) H_2 cm^{-2}.

We adopt i = 37° as the inclination of the galaxy, which is estimated from an axial ratio of the outer envelope of NGC 1068 (Table 1). Then, we have 1.2 × 10^{22} H_2 cm^{-2}, or 200 $M_\odot$ pc^{-2} for the surface density projected on the galactic plane. This value is much larger than the mean surface density 75 $M_\odot$ pc^{-2} of our Galaxy within R = 1.5 kpc evaluated using the data of Sanders, Solomon, and Scoville (1984). If we assume the same scale height of the CO disk as that of the central region in our Galaxy ($z_{HWHM} \sim 40$ pc; Sanders, Solomon, and Scoville 1984), the mean volume density becomes 49 H_2 cm^{-3}. In the region of 1′ × 1′, the total mass of molecular hydrogen is estimated to be $M_{H_2} = 5.6 \times 10^9 M_\odot$.

© American Astronomical Society • Provided by the NASA Astrophysics Data System

1989ApJ...337..691K

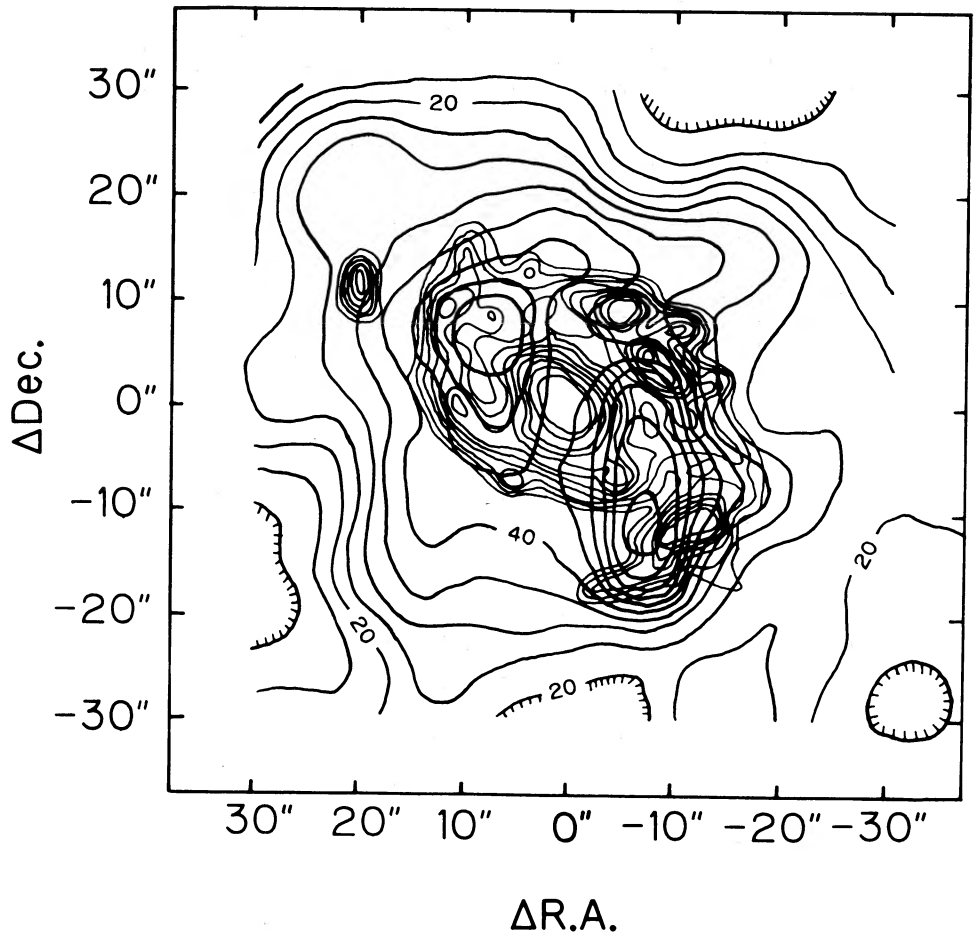

FIG. 4.—Superposition of the integrated intensity map (Fig. 3) on the *U*-band isophotes of the inner arm region. Isophotes are drawn by one of the authors (N. K.) and M. Nishimura and K. Toyama.

Telesco and Harper (1980) estimated the dust mass of $M_d = 2 \times 10^7\ M_\odot$ in almost the same region from far-infrared observations, so that the gas-to-dust ratio is $M_{H_2}/M_{dust} = 300$. This is 3 times as large as the Galactic value (~ 100) but is in the range of infrared bright galaxies (450 ± 270; Young *et al.* 1986). Heckman, Balick, and Sullivan (1978) give $3.5 \times 10^9\ M_\odot$ for the total mass of neutral hydrogen. If the neutral hydrogen is distributed uniformly with radius, we have $M_{H\,I} = 0.1 \times 10^9\ M_\odot$ for the H I mass within the $1' \times 1'$ disk. There is, however, evidence to suggest that in the central region of NGC 1068 the emission of neutral hydrogen is strongly affected by self-absorption (Baan and Haschick 1983), and at present no detailed knowledge is available on the distribution of neutral hydrogen in the $1' \times 1'$ disk.

Assuming a rotation velocity of 266 km s^{-1} from Figure 7, we estimate $4.4 \times 10^{10}\ M_\odot$ for the dynamical mass in the $1' \times 1'$ disk. The H_2 mass estimated above is then 13% of the dynamical mass, which may be a reasonable value.

IV. DISCUSSION

a) *Comparison with the Interferometer Observations*

The present single-dish map (Fig. 3) is very different from the interferometer map of Myers and Scoville (1987), although some similarity is found between them. Our intensity map indicates the extended disk component and the northeast and southwest components, while their interferometer map shows an incomplete molecular ring consisting of two parts.

The southern part of the ring in the interferometer map may correspond to our southeast component. The peak of the southern part nearly agrees with that of the southwest component in our integrated CO map (Fig. 3), and its elongation at (15″ west, 7″ south) just coincides with the northwestward elongation of the southern part of the ring. The velocity structure in the interferometer map is also similar to that of the southwest component shown in Figure 5.

On the other hand, no peak corresponding to that of the northern part of the ring can be found in our intensity map (Fig. 3), and the peak position (3″ west, 16″ north) in the southern part of the ring does not agree with that of our northeast component at (8″ east, 8″ north). The difference in the two peak positions is larger than the pointing error of our data (<4″). Comparison suggests a possibility that the northern part of the ring corresponds to a spiral-like structure ($R \sim 20''$) seen in the northwest quadrant of our intensity map. That no northeast component is resolved in the interferometer map seems to suggest a plateau-like CO distribution in the northeast component. In any case, the differences could be partly attributed to the absence of components of low spatial frequency in the interferometer measurements and to a larger beam of our single-dish observations.

© American Astronomical Society • Provided by the NASA Astrophysics Data System

1989ApJ...337..691K

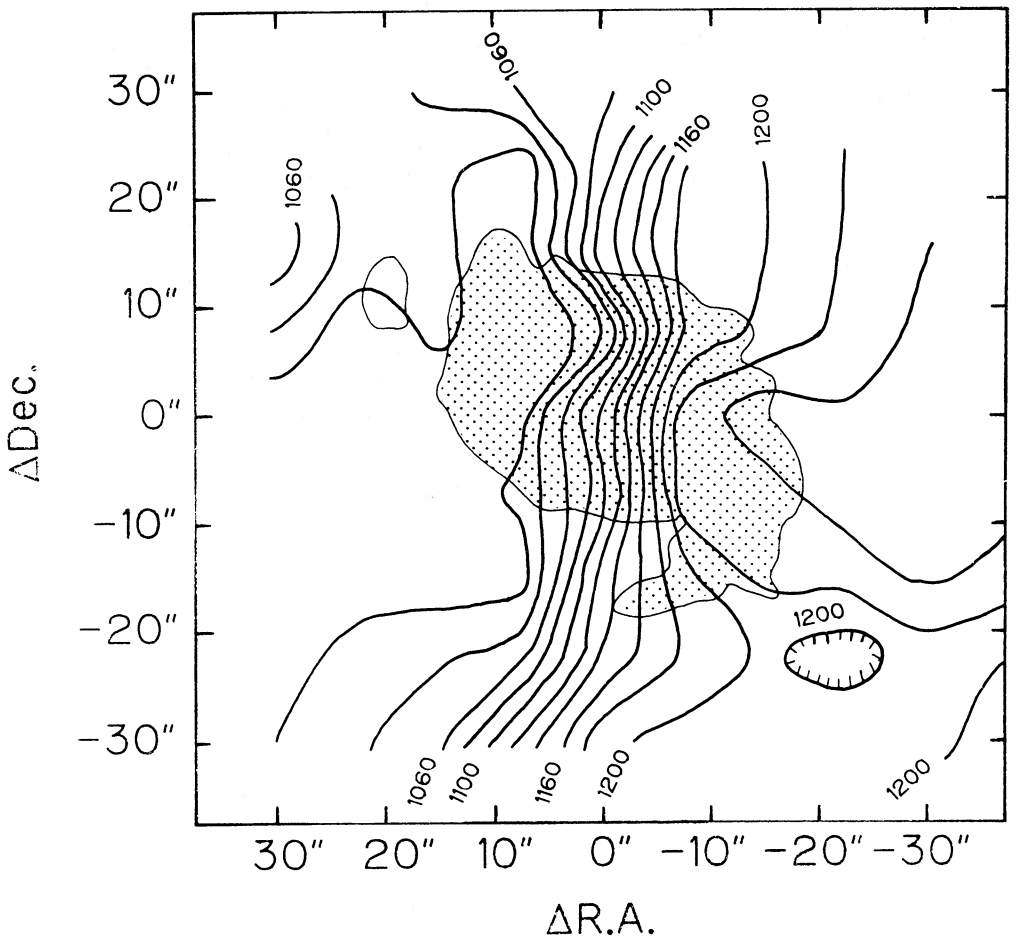

FIG. 5.—Contour map of the peak velocities of CO emission. Velocity structures to indicate the presence of the northeast and southwest components are clearly seen on the map. The map suggests a position angle of 82° for the kinematic major axis.

b) *Comparison with Infrared and Radio Continuum Observations*

Comparison with the radio continuum map of Wynn-Williams, Becklin, and Scoville (1985) shows that the disk component of CO is similar both in shape and size to the radio plateau (~50″ diameter). The observations of NGC 1068 on the Kuiper Airborne Observatory also reveals a far-infrared source the size of which is comparable to that of the CO disk (Telesco *et al.* 1984; Lester *et al.* 1987). As studied in § III*a*, the disk component coincides well with dusty red regions just outside the inner arm region (see Fig. 2 of Ichikawa *et al.* 1987). Baldwin, Wilson, and Whittle (1987) also pointed out the similarity between the radio plateau and the Hβ plateau (Balick and Heckman 1985). It appears likely that the CO disk component, the radio plateau, and the far-infrared source are the emission arising from the same region of star formation.

Blitz, Mathieu, and Bally (1986) have recently studied the correlations between the CO and infrared luminosities for the Seyfert galaxies NGC 1068, NGC 3227, NGC 4051, and NGC 6814. The result shows a good correlation with 100 μm flux, but no good correlation is found between the CO and 10 μm emission. This can be understood if in the last three Seyferts as well as in NGC 1068 the CO emission and 100 μm infrared flux come from the same star-forming region.

The important finding is that there is excellent correspondence between the two northeast and southwest components and the 10 μm sources observed by Telesco *et al.* (1984) (Fig. 8). Examination of the 10 μm map and Table 1 of Telesco *et al.* (1984) reveals two distinct zones having flux densities higher than 100 mJy. One is the zone including the position (9″ east, 9″ north) and its three neighboring positions, which coincides very well with the northeast component of CO. The other is the zone having the highest flux density at the position (12″ west, 6″ south) located on the most heavily obscured portion of a southwest inner spiral, which obviously corresponds to the position of the maximum peak temperature. Except for the nuclear source, regions of intense 10 μm emission correspond not to optically bright regions but to dusty complex ones. We thus conclude that the CO emission from the northeast and southwest components and the 10 μm emission from the above two zones arise from the same dusty molecular clouds embedded within the inner arm region. The most intense bursts of star formation would be taking place in the two regions corresponding to the northeast and southwest components.

Here we point out a difference in the IR and UV properties between the nucleus and the northwest H II complexes (knot 5 of Schild, Tresch-Fienberg, and Huchra 1985). These two are comparable emitters of UV light (Snijders, Briggs, and Boksenberg 1982), and, as is well known, the nucleus of NGC 1068 is a strong IR source. On the other hand, the 10 μm map of Telesco *et al.* (1984) shows no prominent IR emission in the northwest H II complexes. This suggests that the nucleus of NGC 1068 is

© American Astronomical Society • Provided by the NASA Astrophysics Data System

1989ApJ...337..691K

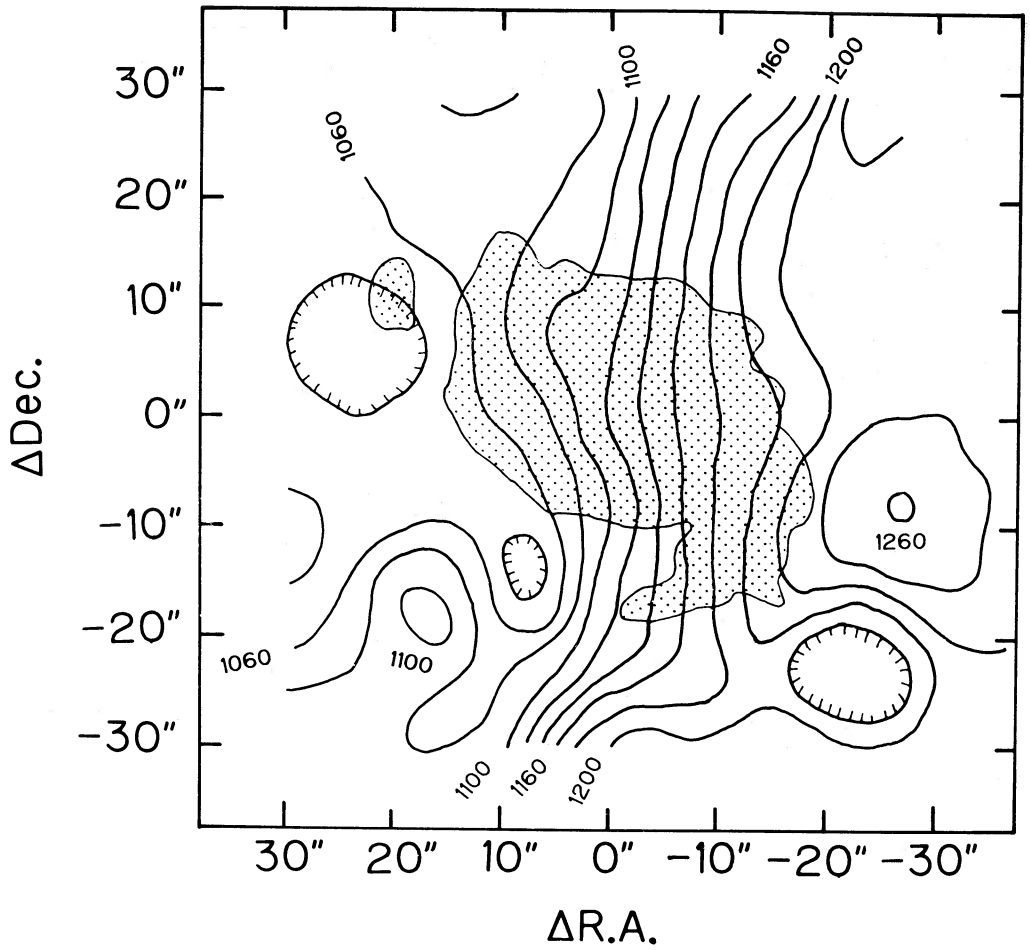

FIG. 6.—Contour map of the mean velocities of CO emission

in a physical state different from that of normal H II regions. Tresch-Fienberg *et al.* (1987) have suggested the possibility that the 10 μm emission from the nucleus is due to the thermal reradiation from dust heated by a nonthermal source.

c) *Gas Kinematics*

Myers and Scoville (1987) have interpreted their velocity contour in terms of the combination of circular rotation and radial expansion motions. The deduced average rotational and expansion velocities are 164 and 71 km s^{-1}, respectively, implying that there are significant noncircular motions in CO molecular gas. This result depends strongly on the inclination and position angle of the major axis adopted, and the inclination $i = 40°$ and the major axis of p.a. 55° (Walker 1968) are used by them.

Expansion motion has the effect of rotating the line of nodes. Therefore, we should find evidence that suggests the expanding motion of a "molecular ring" ($R \sim 15''$) in our velocity contour maps (Figs. 5 and 6), if the interpretation of Myers and Scoville (1987) is correct. However, Figures 5 and 6 exhibit no such velocity structure, and are evidently inconsistent with the position angle of 55° adopted by Myers and Scoville for the major axis, which requires a significant noncircular motion. As mentioned by Myers and Scoville, the major axis of p.a. 83° requires no expansion motion, and a deduced circular velocity becomes 185 km s^{-1}.

The line-of-sight velocity contours are radial about the center for the case in which a rotation velocity is constant, and the contours are perpendicular to the line of nodes for the case in which the rotation velocity is proportional to the radius from the center. The position-velocity map (Fig. 7) suggests that the CO rotation curve increases linearly with the radius from the center and becomes flat at $R \sim 10''$. Therefore, predicted velocity contours should be radial outside the central $\sim 20''$ and parallel to the minor axis inside that central region, if the expanding motion is negligible. Such a prediction is, however, very different from our velocity contour maps (Figs. 5 and 6). This implies that the CO velocity field cannot be interpreted only in terms of a pure circular motion. Larger-scale noncircular motions might be required to explain the peculiar CO velocity field of NGC 1068.

Comparison with the position-velocity map of H I emission in p.a. 70° (Fig. 7 of Baan and Haschick 1983) shows that on the west side the rotation curve remains nearly flat up to $R \lesssim 4'$–$5'$ (21–26 kpc) with $v_{\rm LSR} \approx 1230$ km s^{-1}, while on the east side the rotation curve, whose minimum is 1005 km s^{-1} at $R = 8''$ (700 pc), becomes about 1050 km s^{-1} outside $R \gtrsim 1'$ (5.2 kpc). This implies that in the outer envelope ($R \gtrsim 1'$) the

© American Astronomical Society • Provided by the NASA Astrophysics Data System

1989ApJ...337..691K

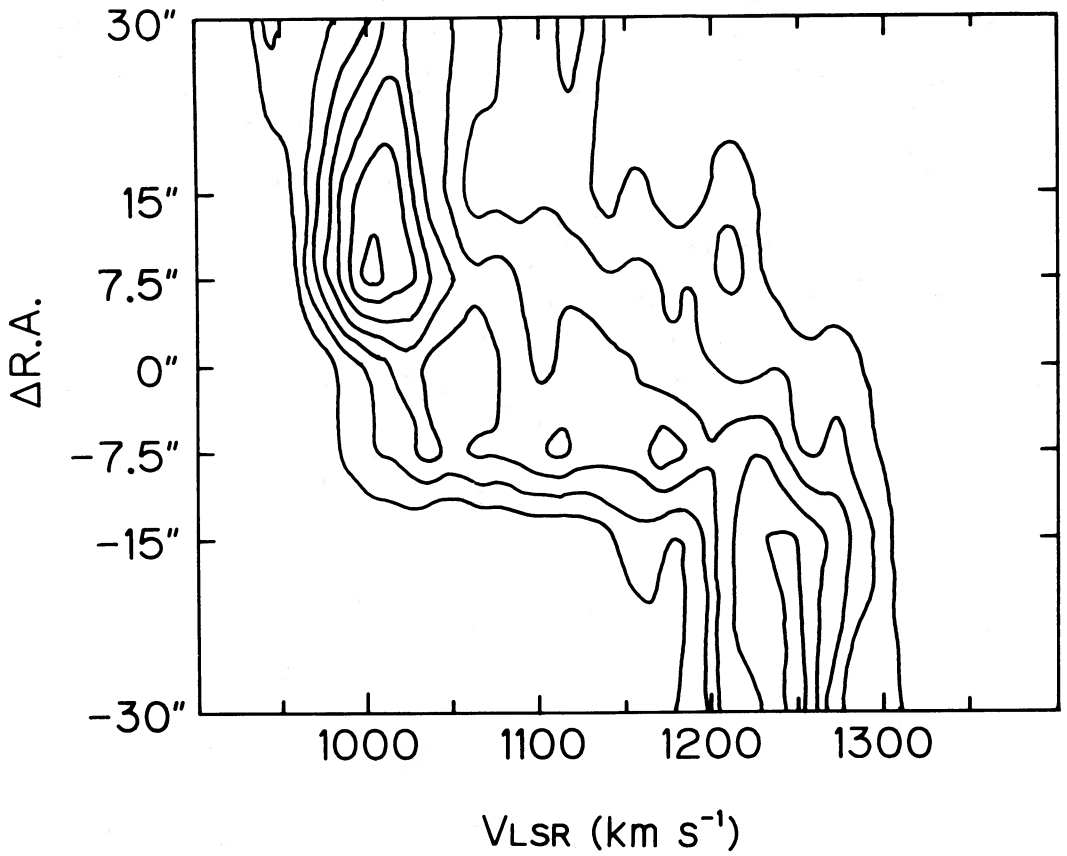

FIG. 7.—Position-velocity diagram of the CO emission along the position angle 90°. The lowest contour level and the contour intervals are 0.065 and 0.052 K, respectively. The intensity is smoothed to 18.2 km s^{-1} resolution. The rotation curve becomes nearly flat at the outside $\sim 10''$ from the center.

velocity field of NGC 1068 is not symmetric with respect to the center. It seems likely that the H I envelope of NGC 1068 is distorted or warped. Further H I and CO observations of the envelope and the disk outside the central $60'' \times 60''$ are needed to understand the gasdynamics of NGC 1068.

d) CO Line-Width Map

As can be seen from Figure 2, the CO line profiles observed are asymmetrically very broad, especially in the central $30'' \times 30''$. The line-width map (Fig. 9) reveals a good coincidence between regions of broad CO line profiles and the northeast and southwest radio lobes (Wilson and Ulvestad 1983, 1987), suggesting a physical relation between the radio lobes and molecular clouds. The map also shows that CO lines broader than 200 km s^{-1} (FWHM) are only observed in the southwest quadrant of the central region, consistent with the Hα observations of Atherton, Reay, and Lucy (1985). The northeast radio lobe appears to correspond to an optical flare emanating from the nucleus in p.a. 30° (Burbidge, Burbidge, and Prendergast 1959; Walker 1968). Comparison with the optical isophotes superposed on Figure 4 shows that the southwest radio lobe ($R \lesssim 8''$–$10''$), which just falls interior to the contour of 200 km s^{-1}, coincides with a southwest extension of optical isophotal contours in which a bright optical knot ($R = 8''$, p.a. = 220°) is seen. Figure 4 also indicates that the optical knot lies near a CO contour of the highest level in the southwest component.

The nuclear source, northeast radio lobe ($R \lesssim 5''$) , and southwest hot spot ($R \approx 5''$) would be the components of a "mini"–double source (Wilson and Ulvestad 1987). If the velocity of the ejecta ranges from 4000 to 15,000 km s^{-1} (Wilson and Ulvestad 1987), the travel time is estimated to range from 12×10^4 to 3×10^4 yr, respectively, for the mini–double source. For the southwest radio lobe, simple calculation gives $H = 9 \times 10^{-5}$ G, $E_e = 7 \times 10^{53}$ ergs, and $E_{\rm tot} = 4 \times 10^{54}$ ergs for the magnetic field strength, the energy of relativistic electrons, and the total energy, respectively, where a spectrum extending from to 10 MHz to 100 GHz with spectral index $\alpha = 1.2$, the ratio of total cosmic-ray energy density to that of the electron $K = 2$, and the equipartition between cosmic-ray and magnetic energy densities are assumed. The magnetic field strength estimated is comparable to that of Cyg A (Hargrave and Ryle 1974), implying that they have similar physical states, though very different in scales and environments. The assumed spectrum gives the radio luminosity $L_R = 5 \times 10^{39}$ ergs s^{-1}, and a lifetime of the source is estimated to be $t_e = E_e/L_R = 4 \times 10^6$ yr. The radio luminosity and magnetic field strength can be explained by a continuous mass-ejection model of Morita (1982), assuming a rate of energy release $L_0 = 10^{42}$ ergs s^{-1}, an ejection rate of mass $\dot{M}_0 = 0.5\ M_\odot\ {\rm yr}^{-1}$, an isothermal gas with the temperature $T_0 = 10^6$ K and a central density $\rho_0 = 15\ {\rm cm}^{-3}$, and a galaxy with total mass $M_* = 10^{10}\ M_\odot$ and core radius $b = 100$ pc. Taking the velocity of 100 km s^{-1} for molecular mass motion, we obtain $2 \times 10^7\ M_\odot$, so that the kinetic energy becomes equal to the total energy of cosmic rays evaluated above. The

© American Astronomical Society • Provided by the NASA Astrophysics Data System

1989ApJ...337..691K

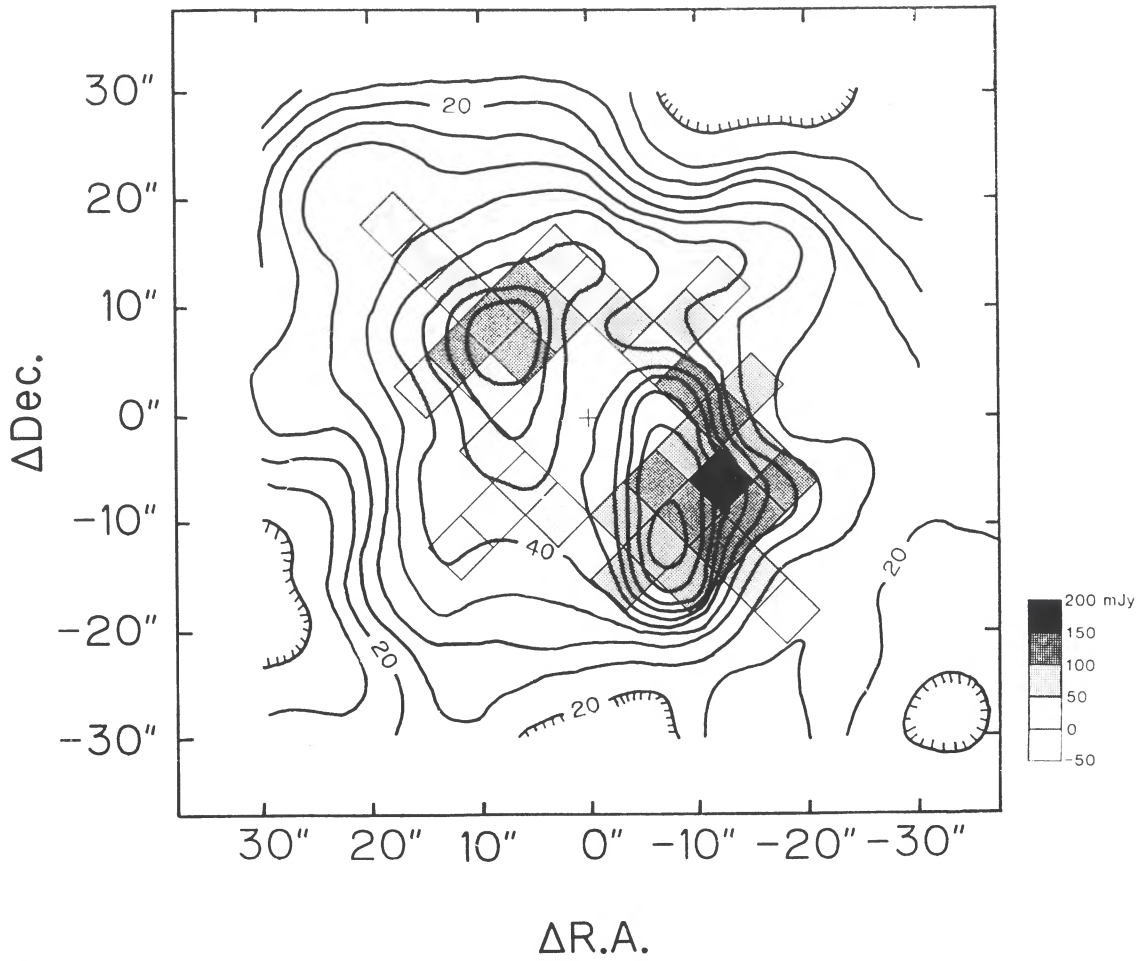

FIG. 8.—Superposition of the CO contour map (Fig. 3) on the 10 μm map of Telesco *et al.* (1984). The northeast and southwest components of CO coincide with regions of strong 10 μm emission.

total momentum of the molecular gas interacting with relativistic plasma is

$$MV \sim 2.0 \times 10^{47}(M/10^7\ M_\odot)(V/100\ \mathrm{km\ s^{-1}})\ \mathrm{g\ cm\ s^{-1}}\ ,$$

where M and V are the mass and velocity of the molecular gas, respectively. On the other hand, the momentum ejected during a time t_0 is

$$M_0 V_0 t_0 \sim 2.5 \times 10^{47}(\dot{M}_0/0.5\ M_\odot\ \mathrm{yr^{-1}})^{1/2} \times (L_0/10^{42}\ \mathrm{ergs\ s^{-1}})^{1/2}(t_0/10^6\ \mathrm{yr})\ \mathrm{g\ cm\ s^{-1}}\ ,$$

where $V_0 = (2L_0/\dot{M}_0)^{1/2}$ is the ejection velocity. Thus, we see that $\dot{M}_0 V_0 t_0 \sim MV$ for $t_0 \sim t_e$.

The nuclear ejecta and their interaction with the ambient gas may be a general phenomenon in nuclear activity: A jetlike expansion of the molecular gas is also suggested in the central part of the Galaxy (Fukui *et al.* 1977). As shown in § III, NGC 1068 has no central concentration of CO emission ($R < 5''$). It is possible to suppose that within a central region of NGC 1068 the molecular gas has been swept out by the nuclear ejecta. Then, we have 9×10^6 yr as the expansion time for $R = 0.5$ kpc at 100 km s^{-1}.

We have no knowledge of actual directions of the nuclear ejecta. If the nuclear clouds (Walker 1968) move together with them, the northeast radio lobe goes backward while the southwest radio lobe goes forward. Projected distances of the radio lobes $R = 5''$–$10''$ correspond to 0.45–0.9 kpc, and NGC 1068 appears nearly face-on ($i = 37°$). Therefore, if the nuclear ejecta are off-plane, the molecular gas would have a three-dimensional structure rather than a thin-disk structure, because the height of the molecular gas from the galactic plane of NGC 1068 might be comparable to the projected scale of radio lobes. This is consistent with the suggestion that the radio plateau is a spherical region (Wynn-Williams, Becklin, and Scoville 1985).

V. CONCLUSION

We have carried out the high-resolution CO observations of the central $60'' \times 60''$ of the Seyfert/starburst galaxy NGC 1068, using the NRO 45 m telescope. The main results are summarized as follows:

1. The CO distribution within the central disk consists of the disk, northeast and southwest components, which are located in optically red, dusty areas. The former coincides with the radio plateau and far-infrared source, and the latter two coincide well with regions of strong 10 μm emission. The CO emission is associated not with ionized gaseous clouds within the luminous inner spirals but with dusty molecular clouds embedded within the central $\sim 1'$.

© American Astronomical Society • Provided by the NASA Astrophysics Data System

1989ApJ...337..691K

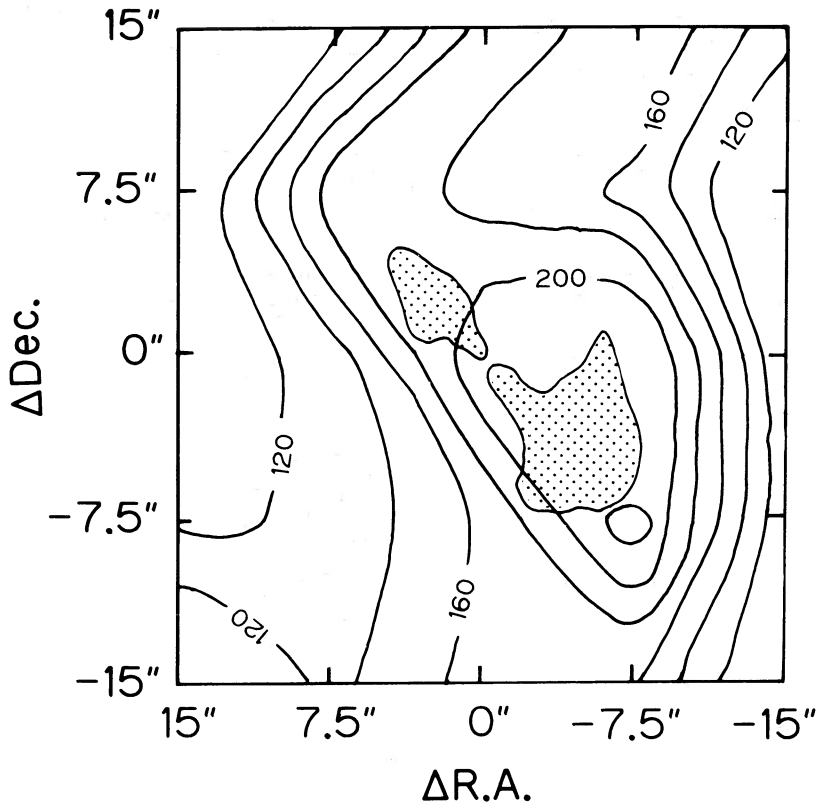

FIG. 9.—Line-width map of CO emission. The line width is defined by $V_{FWHM} = I_{CO}/T_A^*(\text{peak})$. The radio jets (Wilson and Ulvestad 1983) are superposed for comparison.

2. The total H_2 mass is estimated to be $5.6 \times 10^9\ M_\odot$. The deduced molecular mass is about 13% of the dynamical mass within the central $1' \times 1'$.

3. The CO velocity field reveals a peculiar structure in that the isovelocity contours run primarily parallel to the position angle of 82°. The velocity contours cannot be explained only in terms of a circular motion, implying that there are large-scale noncircular motions in the CO molecular clouds.

4. The CO line-width map reveals a good coincidence between regions of broad CO line profiles and the northeast and southwest radio lobes, suggesting a physical relation between the molecular gas and relativistic plasma in the radio lobes.

We are grateful to the staff of the Nobeyama Radio Observatory for help with the observations. We wish to thank S. Okamura and S. Ichikawa for supplying the isophotes of NGC 1068 and the Kiso Schmidt photographs of NGC 1068.

REFERENCES

Antonucci, R. R. J., and Miller, J. S. 1985, *Ap. J.*, **297**, 621.
Arp, H. 1966, *Atlas of Peculiar Galaxies* (Pasadena: California Institute of Technology).
Atherton, P. D., Reay, N. K., and Taylor, K. 1985, *M.N.R.A.S.*, **216**, 17P.
Baan, W. A., and Haschick, A. D. 1983, *A.J.*, **88**, 1088.
Baldwin, J., Wilson, A. E., and Whittle, M. 1987, *Ap. J.*, **319**, 84.
Balick, B., and Heckman, T. 1985, *A.J.*, **90**, 197.
Blitz, L., Mathieu, R. D., and Bally, J. 1986, *Ap. J.*, **311**, 142.
Burbidge, E. M., Burbidge, G. R., and Prendergast, K. H. 1959, *Ap. J.*, **130**, 26.
Clements, E. D. 1981, *M.N.R.A.S.*, **197**, 829.
Evans, I. N., and Dopita, M. A. 1986, *Ap. J. (Letters)*, **320**, L15.
———. 1987, *Ap. J.*, **319**, 662.
Fukui, Y., Iguchi, T., Kaifu, N., Chikada, Y., Morimoto, M., Nagane, K., and Miyaji, K. 1977, *Pub. Astr. Soc. Japan*, **29**, 643.
Hargrave, P. J., and Ryle, M. 1974, *M.N.R.A.S.*, **166**, 305.
Heckman, T. M., Balick, B., and Sullivan, W. T., III. 1978, *Ap. J.*, **224**, 745.
Ichikawa, S., Okamura, S., Kaneko, N., Nishimura, M., and Toyama, K. 1987, *Pub. Astr. Soc. Japan*, **39**, 411.
Keel, W. C., and Weedman, D. W. 1978, *A.J.*, **83**, 1.
Khachikian, E. Ye., and Weedman, D. W. 1971, *Astrofizika*, **7**, 389.
Lester, D. F., Joy, M., Harvey, P. M., Ellis, H. B., Jr., and Parmar, P. S. 1987, *Ap. J.*, **321**, 755.
Morita, K. 1982, *Pub. Astr. Soc. Japan*, **34**, 65.
Myers, S. T., and Scoville, N. Z. 1987, *Ap. J. (Letters)*, **312**, L39.
Nishimura, M., Kaneko, N., and Toyama, K. 1984, *Astr. Ap.*, **130**, 46.
Rickard, L. J., Palmer, P., Morris, M., Turner, B. E., and Zuckerman, B. 1977, *Ap. J.*, **213**, 673.
Rubin, V. C., Burstein, D., Ford, W. K., Jr., and Thonnard, N. 1985, *Ap. J.*, **289**, 81.
Rubin, V. C., Ford, W. K., Jr., Thonnard, N., and Burstein, D. 1982, *Ap. J.*, **261**, 439.
Sandage, A. 1961, *The Hubble Atlas of Galaxies* (Washington, DC: Carnegie Institution of Washington).
Sandage, A., and Tammann, G. A. 1975, *Ap. J.*, **196**, 313.
Sanders, D. B., Solomon, P. M., and Scoville, N. Z. 1984, *Ap. J.*, **276**, 182.
Schild, R., Tresch-Fienberg, R., and Huchra, J. 1985, *A.J.*, **90**, 441.
Scoville, N. Z., Young, J. S., and Lucy, L. B. 1983, *Ap. J.*, **270**, 443.
Smith, M. G., Weedman, D. W., and Spinrad, H. 1972, *Ap. Letters*, **11**, 21.
Snijders, M. A. J., Briggs, S. A., and Boksenberg, A. 1982, *Proc. Third European IUE Conf.*, ed. E. Rolfe, A. Heck, and B. Battrick (Madrid: ESA), p. 551.
Snijders, M. A. J., Netzer, H., and Boksenberg, A. 1986, *M.N.R.A.S.*, **222**, 549.
Telesco, C. M., Becklin, E. E., Wynn-Williams, C. G., and Harper, D. A. 1984, *Ap. J.*, **282**, 427.
Telesco, C. M., and Harper, D. A. 1980, *Ap. J.*, **235**, 392.
Tresch-Fienberg, R., Fazio, G. G., Gezari, D. Y., Hoffman, W. F., Lamb, G. M., Shu, P. K., and McCreight, C. R. 1987, *Ap. J.*, **312**, 542.
Ulrich, B. L., and Haas, R. W. 1976, *Ap. J. Suppl.*, **30**, 247.
Walker, M. F. 1968, *Ap. J.*, **151**, 71.

© American Astronomical Society • Provided by the NASA Astrophysics Data System

1989ApJ...337..691K

Weedman, D. W. 1973, *Ap. J.*, **183**, 29.
Wilson, A. S., and Ulvestad, J. S. 1982, *Ap. J.*, **263**, 576.
———. 1983, *Ap. J.*, **275**, 8.
———. 1987, *Ap. J.*, **319**, 105.
Wynn-Williams, C. G., Becklin, E. E., and Scoville, N. Z. 1985, *Ap. J.*, **297**, 607.
Young, J. S., Schloerb, P., Kenney, J. D., and Lord, S. D. 1986, *Ap. J.*, **309**, 443.
Young, J. S., and Scoville, N. Z. 1982, *Ap. J.*, **258**, 467.

YASUO FUKUI and TAKAHIRO IWATA: Department of Astrophysics, Nagoya University, Chikusa-ku, Nagoya 464, Japan

NOBORU KANEKO and KAZUHIKO MORITA: Department of Physics, Faculty of Science, Hokkaido University, Sapporo 060, Japan

HARVEY S. LISZT: National Radio Astronomy Observatory, Edgemont Road, Charlottesville, VA 22901

NAOMASA NAKAI and NORIO KAIFU: Nobeyama Radio Observatory, Minamimaki-mura, Minamisaku-gun, Nagano 384-13, Japan

KOJI SUGITANI: Department of General Education, Nagoya City University, Mizuho-ku, Nagoya 467, Japan

© American Astronomical Society • Provided by the NASA Astrophysics Data System